The dual-band NIKA: Technical Note on Calibration v2

A. Monfardini, A. Benoit, A. Bideaud, F. X. Désert, J. Macias-Perez

June 17, 2011

Institut Néel (IN) MCBT, BP 166, 38042 Grenoble, France, Institut de Planétologie et d'Astrophysique de Grenoble (IPAG), BP 53, 38041 Grenoble, France , Laboratoire de Physique Subatomique et de Cosmologie (LPSC), 53 rue des Martyrs, 38026 Grenoble,

Abstract

We detail the procedure to start from the raw NIKA data and to obtain a signal that can be calibrated, i.e. a signal that is supposed to be linear with the absorbed number of photons. This applies to the 2010 October campaign configuration. This note is an abridged/augmented version of a section of an article (Monfardini et al 2011, to be submitted).

Superconducting detectors – data reduction – kinetic-inductance – resonators – multiplexing – large arrays

Introduction

A KID is designed to resonate from 1 to 10 GHz and exhibits a loaded quality factor exceeding $Q_L > 10^5$. Thus each KID occupies a bandwidth of order $\Delta f = f/Q_L$ ~10-100 kHz. Similar to standard lock-in techniques, the readout allows 112 separate measurement tones to be generated and simultaneously monitored (for band A (1mm) and band B (2 mm) independently) within the IF measurement bandwidth. A KID delivers a raw signal as the result of a lockin signal I and a quadrature signal Q at a fixed but parametrable frequency that we note f_i for a given i kid.

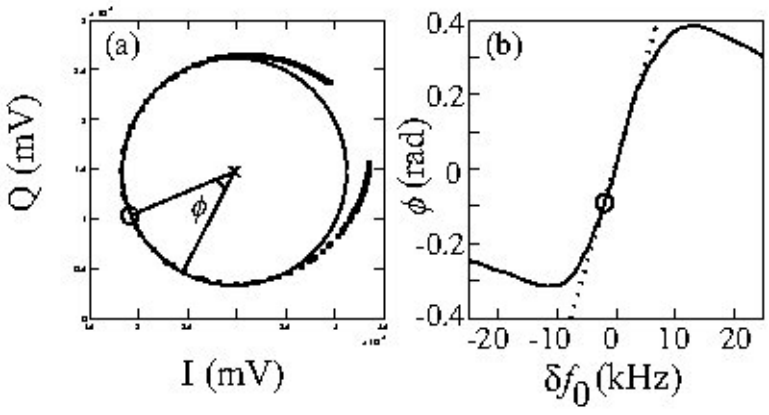

Figure 1: (a, left) Location of (I, Q) points in the complex plane as measured during a frequency sweep. (b, right) Corresponding complex phase versus frequency during the same scan.

Currently, the LEKID array (Band B) operates in the frequency range 1.27-1.45 GHz. Within this bandwidth, 104 pixels and 8 off-resonance blind tones could be used for measurement. The antenna-coupled KID array (Band A) has a central pixel core operating at 5-5.2 GHz. Due to the larger inter-resonator frequency spacing of this array, only 72 core pixels could be simultaneously measured out of the total 256 pixels in the array.

The response of every pixel in an array is measured simultaneously and broadcast via UDP packets by the ROACH electronics to the control computers at a rate of 22 Hz. The individual pixel responses are composed of a pair of in-phase (I) and quadrature (Q) values which result from the final stage of digital mixing and low-pass filtering. Theses values can be translated into the traditional transmission phase (hereafter called raw phase) and amplitude (the raw amplitude) using the identities $\theta = \arctan(Q/I)$ and $A^2 = I^2 + Q^2$. An alternative approach is to plot these values in the complex plane. An example of a standard frequency sweep around a resonance is provided in Fig. 1a. Small changes in illumination result primarily in motion around this curve and thus it is convenient to define a new angle ϕ (the complex phase) about the center of curvature

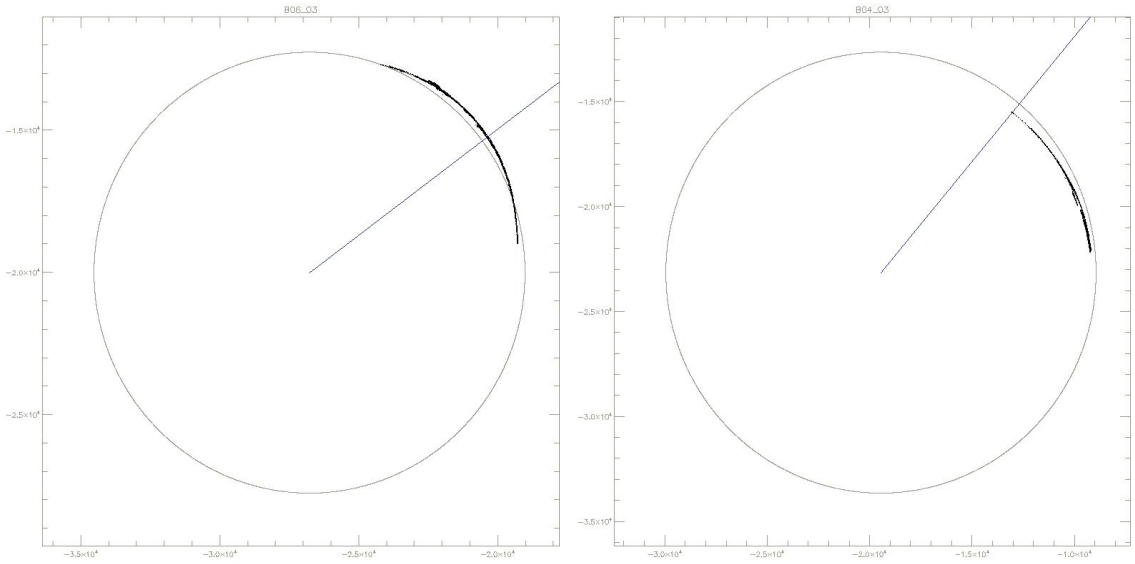

Figure 2: Location of (I, Q) points in the complex plane as measured during a scan on Mars for two detectors. The circle is the fit to a preceding frequency sweep. The straight line goes from the circle center to the origin and indicates ϕ_0 the zero of the complex phase. The two plots are for two B KIDs.

(I_c, Q_c):

$$\phi = \arctan\left(\frac{Q - Q_c}{I - I_c}\right) - \phi_0 \tag{1}$$

where ϕ_0 rotates the plane such that the curve intersects the x axis at the resonance frequency f_0. This is illustrated in

For low intensity radiation, the density of photo-generated quasiparticles in a KID is proportional to the incident photon flux. To first order, this results in a linear shift in the kinetic inductance and a subsequent linear shift in the resonance frequency ([**?**]). That is:

$$\delta f_{res} = -C f_{res}^3 \delta L_K \propto \frac{f_{res}^3}{n_s} \delta P_i \tag{2}$$

where C is a constant, n_s is the Cooper pair density, and δP_i is the incident power producing a change in kinetic inductance δL_K. A plot of the phase ϕ versus the frequency shift from resonance δf_{res} for a typical KID is shown in Fig. 1b along with the maximum frequency shift during a transit of Mars. From this plot, it is clear that $\partial\phi/\partial f$ is approximately constant for all relevant astronomical signals. Thus $\phi \propto \delta P_i$ with the constant of proportionality being determined during a calibration scan (e.g. on a planet). One caveat is that under large background changes, which can result from weather changes or telescope repointing, n_s changes substantially and causes a significant shift in f_{res}. For this reason, an automatic procedure was implemented to properly determine (I_c, Q_c), ϕ_0 and $\partial\phi/\partial f\ |_{f_0}$ before every scan taken on the telescope to assure

that the measurement would remain in the dynamic range of the KIDs. A given measurement can be converted into a complex phase using Eq. 1 and then converted to an effective frequency:

$$\delta f_0 = \frac{\phi}{\partial\phi/\partial f \mid_{f_0}} \tag{3}$$

In practice, data for a given scan and a given KID include the time stream (22 samples per second) for I, Q, ϕ , δf_0, the 2 latter being calibrated on the circle obtained with the most recent frequency sweep. It also include parameters (fixed for a given scan) giving the circle center (I_c, Q_c), the maximum resonance point ($I(f_0)$, $Q(f_0)$) and the linearized response $\partial\phi/\partial f \mid_{f_0}$. In the version 1 of the data internal calibration, δf_0 is assumed to be linear with the absorbed power.

Version 2 calibration

During the October 2010, we have noticed photometric inconsistencies at the level of 20 to 30 % when repeating measurements of planets or quasars and applying version 1 calibration on a per KID basis. It is less dramatic when averaging 50 to 100 of them. But this hides the problem somehow. We think that that can be solved simply by relaxing the linearization made in Eq. 3. Using the formalism shown by Barends (arXiv 0802:0640), the complex response (similar to $I + jQ$) can be written as:

$$S_{21} = \frac{2Z_{res}Z_0}{Z_{res}\left[2Z_0 + j(X_1 + X_2)\right] + (Z_0 + jX_1)(Z_0 + jX_2)} \tag{4}$$

where Z_0, X_1 and X_2 are real numbers and

$$Z_{res} = \frac{Z_0 Q_e}{2Q_i}\left[1 + 2jQ_i\frac{\Delta f}{f_{abs}}\right] \tag{5}$$

where Q_e and Q_i are (real) quality factors. We now show that in the limit of $X \ll Z_0$, the complex response describes a circle as a function of the frequency $\Delta f = f - f_{abs}$ where f_{abs} is a reference frequency (say without background). In that case, S_{21} can be recast into this form:

$$S_{21} = 1 - \frac{1}{a + jb\Delta f} , \tag{6}$$

with $a = \frac{Q_e}{Q_i}$ and $b = \frac{Q_e}{f_0}$ being real variables. It can be easily shown that the inverse of a complex number with only its imaginary part varying lies on a circle. Hence, the complex response lies approximately on a circle. Going one step further, let's write this complex number

$$z = a + jb\Delta f = r\, e^{j\alpha} , \tag{7}$$

so that

$$S_{21} = 1 - \frac{1}{z} = (1 - \frac{1}{2a}) - \frac{1}{2a}e^{-2j\alpha} , \tag{8}$$

which shows the simple relationship between the complex phase in the circle and the phase of the variable z:

$$\phi = -2\alpha + \phi_1 , \tag{9}$$

where ϕ_1 allows us to account for a phase shift in the transmission line (basically going from S_{21} to the measured complex $I + jQ$). Defining the width of the line as

$$\delta f = \frac{f_0}{2Q_i} ,$$

Eq. 9 can be transformed into

$$f - f_0 = -2\delta f \ \tan\left(\frac{\phi - \phi_1}{2}\right) + f_a , \tag{10}$$

where ϕ_1 can be generally different from the phase ϕ_0 as defined in Eq. 1 with :

$$\phi_0 - \phi_1 = 2 \ \arctan\left[\frac{f_a}{2\delta f}\right] . \tag{11}$$

The interpretation of ϕ_1 can be made more explicit by writing the speed of phase change relative to a frequency change (obtained by derivating Eq. 10):

$$\frac{d\phi}{df} = \frac{1}{\delta f} \cos^2\left[\frac{\phi - \phi_1}{2}\right] . \tag{12}$$

The speed has a maximum value of $\frac{1}{\delta f}$ when the phase is ϕ_1. The resonance frequency ($\phi = \phi_0$) is not necessarily the "best" frequency ($\phi = \phi_1$) at which the sensitivity is maximum. Note that the speed is no longer constant as was assumed in the version 1 calibration scheme (Eq. 3). The version 1 assumption is true only for small phase variations (relative to one radian).

We can express the inverse of the speed as a function of the measured frequency with this formula:

$$\frac{df}{d\phi} = \delta f + \frac{[f - f_1]^2}{4\delta f} , \tag{13}$$

where $f_1 = f_0 + f_a$ is the frequency of maximum speed.

Examples

Let us now show that the version 2 formalism bears some resemblance to what is effectively measured. In a frequency scan, we make a non-linear fit (with the IDL Mpfit routines) using the model:

$$\phi = \phi_1 + 2 \ \arctan \frac{f - f_1}{\delta f} , \tag{14}$$

by finding the 3 parameters ϕ_1, f_1, and δf.

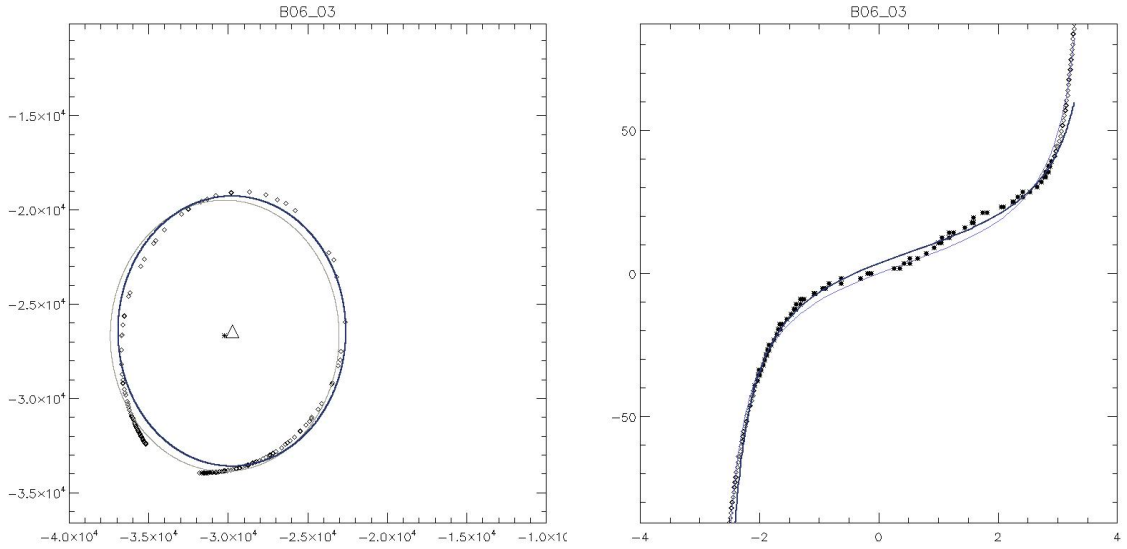

Figure 3: (Left) I, Q trajectory in a frequency scan. The best fit circle is shown in blue. (Right) Relative frequency (in Hz) with respect to the phase (radian). The phase is relative to the resonance frequency. The blue line gives the best fit using Eq. 14.

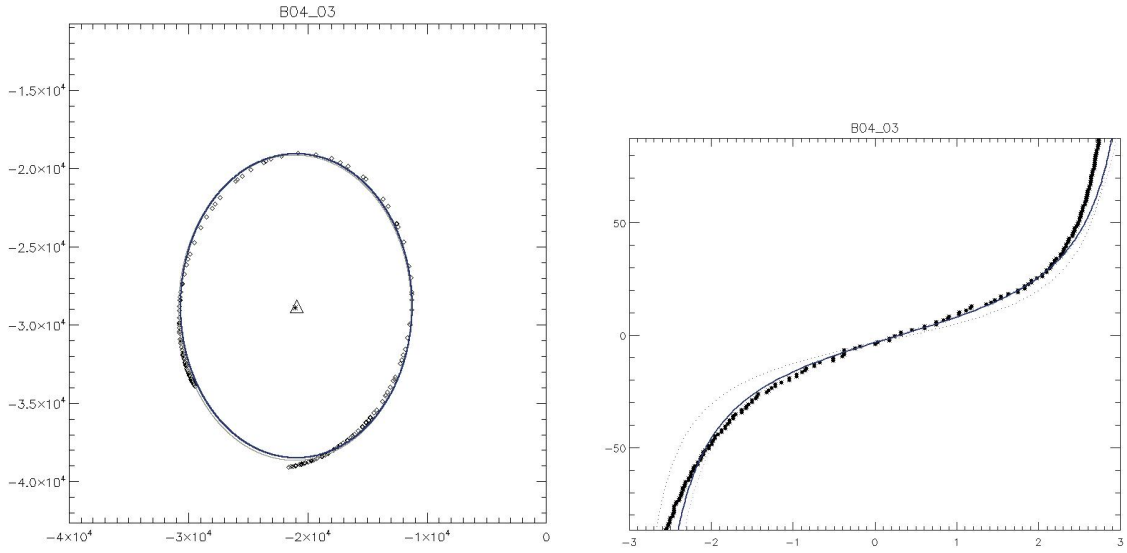

Figure 4: Same as previous figure for another Kid.

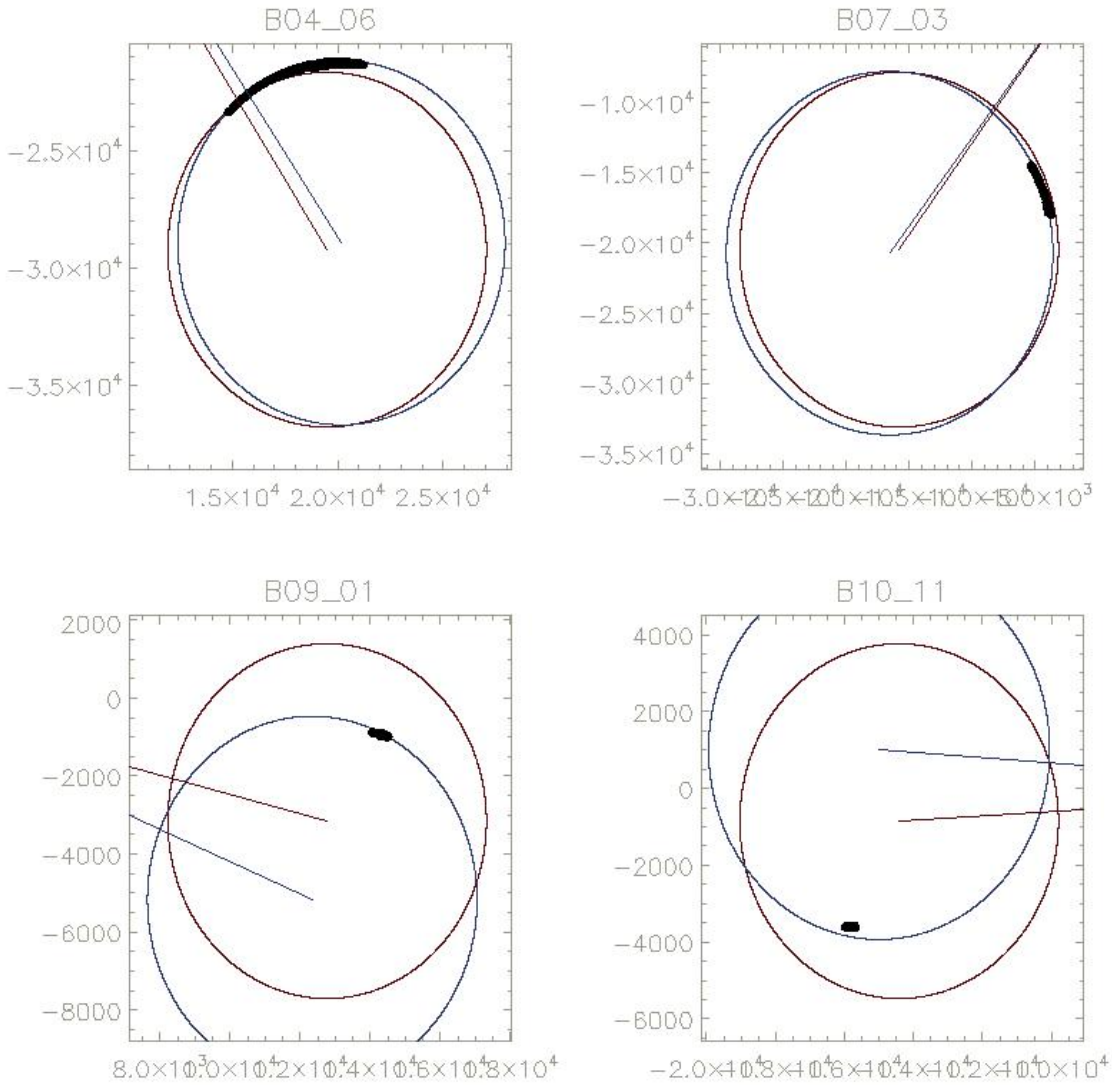

Figure 5: For 4 KIDs we show the circle (brown one) fitted on frequency sweeps. The thick dots are actual measurement on the Mars mapping just following the sweeps. (The black circle correspond to a fit at a different epoch). That the dots follow the fit circles is a consistency check of this calibration scheme.